The HKU Scholars Hub   The University of Hong Kong   香港大學學術庫

Title	**Shear stiffness of granular material at small strains: does it depend on grain size?**
Author(s)	**Yang, J; Gu, X**
Citation	**Géotechnique, 2013, v. 63 n. 2, p. 165-179**
Issued Date	**2013**
URL	**http://hdl.handle.net/10722/188909**
Rights	**Creative Commons: Attribution 3.0 Hong Kong License**

Shear stiffness of granular material at small strains: does it depend on grain size?

J. YANG* and X. Q. GU*

The shear stiffness of granular material at small strain levels is a subject of both theoretical and practical interest. This paper poses two fundamental questions that appear to be interrelated: (a) whether this stiffness property is dependent on particle size; and (b) whether the effect of testing method exists in terms of laboratory measurements using resonant column (RC) and bender element (BE) tests. For three uniformly graded types of glass beads of different mean sizes (0·195 mm, 0·920 mm and 1·750 mm), laboratory tests were conducted at a range of confining stresses and void ratios, using an apparatus that incorporates both RC and BE functions and thus allows reliable and insightful comparisons. It is shown that the small-strain stiffness, determined by either the RC or BE tests, does not vary appreciably with particle size, and it may be practically assumed to be size independent. The laboratory experiments also indicate that the BE measurements of small-strain stiffness are comparable to the corresponding RC measurements, with differences of less than 10%. Furthermore, the BE measurements for fine glass beads are found to be consistently higher than the RC measurements, especially at large stress levels, whereas this feature becomes less evident for medium-coarse glass beads, and eventually diminishes for coarse glass beads. The study indicates that the characteristics of output signals in BE tests can be largely affected by the frequency of the input signal, the mean particle size of the material and the confining stress level, and that these factors are interrelated. Improper interpretation of wave signals may lead to shear stiffness measurements that are unreasonably low, either showing a substantial increase with particle size or showing the opposite. A micromechanics-based analysis assuming the Hertz–Mindlin contact law is presented to offer an understanding of the size effect from the grain scale.

KEYWORDS: dynamics; elasticity; laboratory equipment; laboratory tests; stiffness

INTRODUCTION

The shear stiffness of granular soils at strain levels less than 0·001% – usually denoted as G_0 or G_{max} – is a key parameter in major geotechnical applications involving deep excavations and tunnels, liquefaction evaluation or earthquake ground response analysis. Extensive research has been carried out to study this property, mainly through well-controlled laboratory experiments, particularly using resonant column (RC) tests as they offer high reliability and accuracy at this small strain level (Hardin & Richart, 1963; Iwasaki & Tatsuoka, 1977; Chung *et al.*, 1984; Lo Presti *et al.*, 1997). Of the factors identified as affecting shear stiffness, confining stress and void ratio are recognised to be the main ones. They are now commonly accounted for using an empirical formula taking the form

$$G_0 = AF(e)\left(\frac{\sigma'}{p_a}\right)^n \tag{1}$$

where G_0 is in MPa; σ' is the effective confining stress in kPa; p_a is a reference stress, usually taken as the atmospheric pressure; A and n are two best-fit parameters; and $F(e)$ is a function of void ratio (e) with a typical form of (e.g. Hardin & Richart, 1963; Iwasaki & Tatsuoka, 1977)

$$F(e) = \frac{(2\cdot17 - e)^2}{1 + e} \tag{2}$$

Recent notable work using the resonant column technique includes that by Wichtmann & Triantafyllidis (2009), who conducted a structured programme of resonant column (RC) tests to examine the effect of particle-size distribution on the stiffness of sand. Their data showed that the value of G_0 decreased markedly as the coefficient of uniformity ($C_u = D_{60}/D_{10}$) of sand increased, where D_{60} and D_{10} represent the particle sizes that 60% and 10% of the sand mass are smaller than, respectively. This result is in agreement with that of Iwasaki & Tatsuoka (1977), which was also derived from a number of RC tests on sand. The experimental data also suggested that the small-strain stiffness was independent of the mean particle size of sand (D_{50}).

Bender element (BE) tests, which involve direct measurement of shear waves, have become a promising alternative in recent years for laboratory determination of G_0 values of soils (Dyvik & Madshus, 1985; Viggiani & Atkinson, 1995; Brignoli *et al.*, 1996; Yamashita *et al.*, 2009; Clayton, 2011). A significant advantage of this technique is that it can be incorporated in standard soil mechanics apparatuses such as triaxial and oedometer devices, and the approaches for data interpretation are relatively simple. Relying on this technique, Patel *et al.* (2008) measured the shear wave velocity (V_s) in assemblies of glass beads of different sizes. Their tests indicated that V_s increased as the mean particle size of glass beads decreased, as shown in Fig. 1(a). At the confining stress of 100 kPa, the V_s of glass beads with a mean diameter of 0·5 mm was determined to be 320 m/s, which was about 45% higher than that of glass beads with a mean diameter of 2·5 mm. In terms of shear modulus, the G_0

value of the small-sized glass beads was about 110% higher than that of the large-sized glass beads.

The experimental work of Patel *et al.* (2008), showing an appreciable size dependence of small-strain stiffness, does not agree with that of Wichtmann & Triantafyllidis (2009) and Iwasaki & Tatsuoka (1977). It does, however, appear to be consistent with that of Bartake & Singh (2007), who performed BE tests on three dry sands with similar gradation and found that the G_0 value increased as the mean particle size (D_{50}) of the sand decreased. The work of Sharifipour *et al.* (2004), also using the BE technique to measure the shear wave velocity in glass beads, adds further uncertainty: for glass beads of three different nominal sizes (1·0, 2·0 and 3·0 mm), they obtained an opposite result, showing that the value of V_s increased with increasing particle size, as shown in Fig. 1(b). In terms of shear modulus, 3·0 mm glass beads at a confining stress of 100 kPa were determined to have a G_0 value of about 111·2 MPa, being 66% larger than that of 1·0 mm glass beads.

Evidently, the issue of whether the small-strain shear stiffness is size dependent remains inconclusive and open to discussion. Also, the experimental data from BE tests in the literature seem always to indicate that particle size has an effect on small-strain shear stiffness (although opposite trends were observed in the G_0 variation with grain size), whereas the RC test data seem always to suggest that there is not any size effect. In this respect, an additional question arises: does the testing method have any effect on small-strain stiffness? In RC tests, a soil specimen is subjected to torsional excitation typically at frequencies of several tens of Hz, and the shear stiffness (G_0) is estimated from the measured resonant frequency. In BE tests, however, the shear wave velocity in a soil specimen (V_s) is measured directly

through a pair of piezoelectric transducers at frequencies from several to a few tens of kHz, and is then converted to the shear modulus by $G_0 = \rho(V_s)^2$, where ρ is the mass density of the soil. The two methods indeed involve different principles and interpretations.

With the aim of addressing these two fundamentally important questions, a specifically designed experimental programme has been carried out using an apparatus that incorporates both RC and BE features. The apparatus allows the BE and RC tests to be performed on an identical specimen, thus affording more reliable and convincing comparisons; this is both necessary and desirable, given the observed discrepancies between the RC and BE measurements. Three types of glass beads with different mean particle sizes (D_{50}) but the same uniformity (C_u) were prepared and used as analogue granular soils in the experiment. Their simple and spherical geometry, together with the same uniformity, allowed the influences of particle shape (Cho *et al.*, 2006) and particle size distribution (Wichtmann & Triantafyllidis, 2009) to be isolated, so that any observed difference is attributable to the difference in particle size. This paper presents the main results of this experimental work. Moreover, efforts are made here to explore the possible causes of the contradictory results in the literature through a comprehensive analysis of the experimental data. A grain-scale model is also presented to provide an understanding from the micromechanical point of view.

TEST EQUIPMENT AND MATERIAL
Equipment set-up
The overall set-up of the apparatus is schematically shown in Fig. 2, with close-up views of the key components given in Fig. 3. The apparatus has both RC and BE features and a robust signal conditioning and data acquisition system, along with an environmental chamber. It can accommodate a soil specimen 50 mm in diameter and 100 mm high, with an air-filled cell pressure up to 1 MPa. The resonant column is of bottom-fixed and top-free configuration (the Stokoe type). Compared with the free–free configuration, the fixed–free configuration has the advantages of relatively high available torque and convenient access to the specimen for control of effective stress. A careful calibration of the equipment was carried out using three aluminium bars of different dimensions to establish a calibration curve for the frequency-dependent mass polar moment of inertia of the drive head. Attention should be paid to specimen fixity when testing very stiff materials such as highly cemented sand or weak rock; more details of this issue are beyond the scope of this paper but can be found in, for example, Clayton *et al.* (2009).

To allow for the pulse test in the same system, a pair of bender elements has been instrumented, as shown in Fig. 3. Unlike the conventional design, this single pair of bender elements is able to generate not only shear waves (i.e. S-waves) but also compression waves (i.e. P-waves); this has been achieved by modifying the wiring configuration of the bender elements (Lings & Greening, 2001). Measuring the compression wave can facilitate the interpretation of shear wave signals in situations where the so-called near-field effect is complicated, and it may also serve as a promising alternative for checking the degree of saturation of soil specimens (Yang, 2002). A careful calibration of the pulse testing system was carried out by putting the tips of the two bender elements in direct contact to determine the system delay, including the response time of bender elements and the travel time in the cables. The phase relationship (i.e. initial polarisations) between the input and output signals was also checked in the calibration.
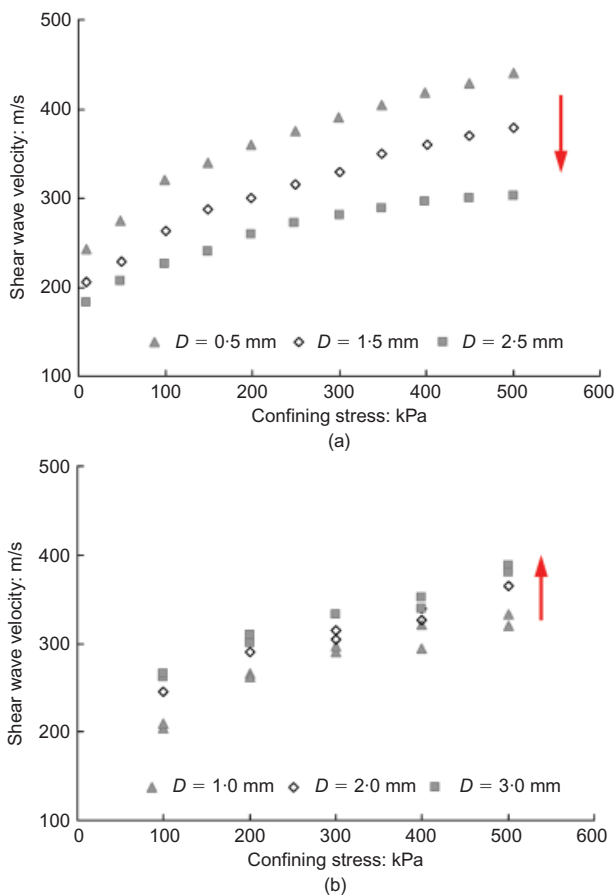

Fig. 1. Test data on shear wave velocity in glass beads of different sizes: (a) Patel *et al.* (2008); (b) Sharifipour *et al.* (2004)
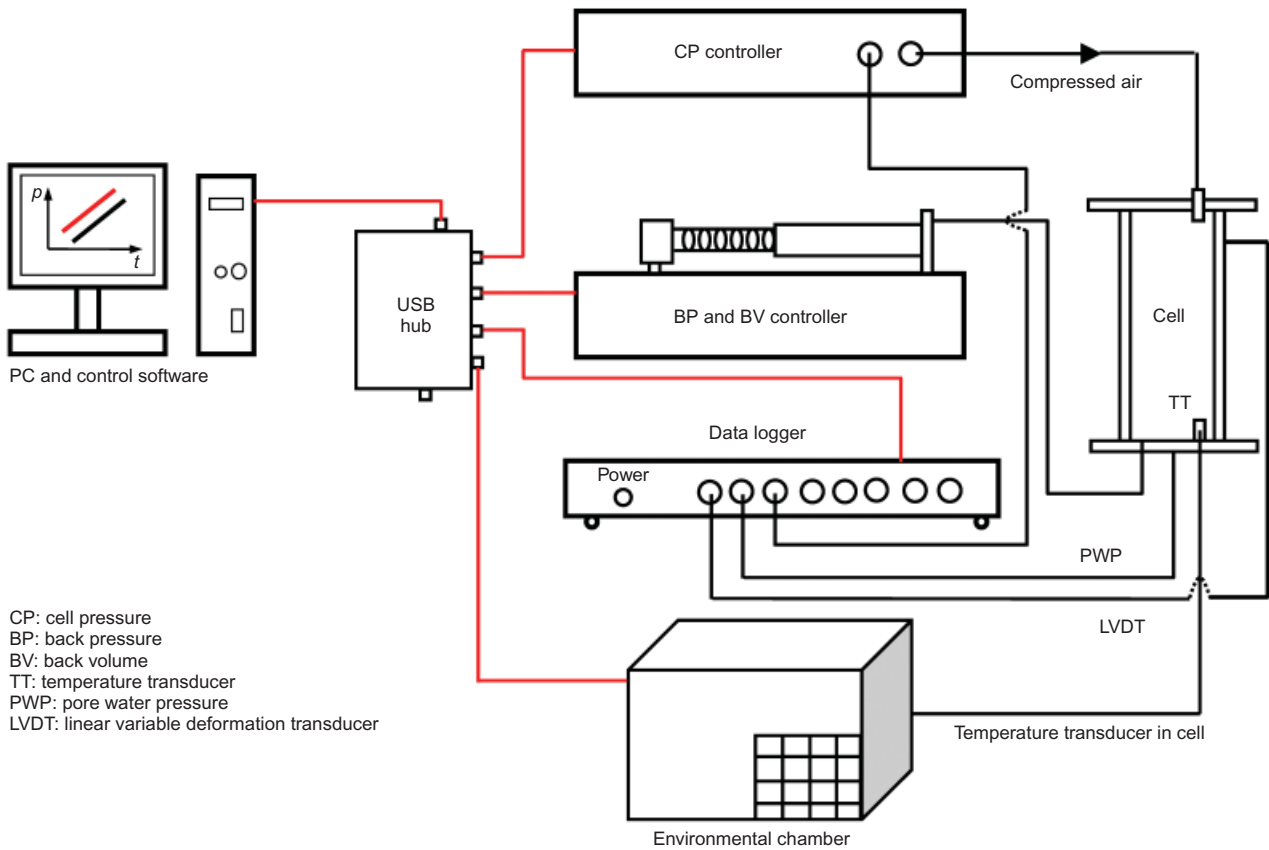
Fig. 2. Set-up of dynamic testing system at The University of Hong Kong

CP: cell pressure
BP: back pressure
BV: back volume
TT: temperature transducer
PWP: pore water pressure
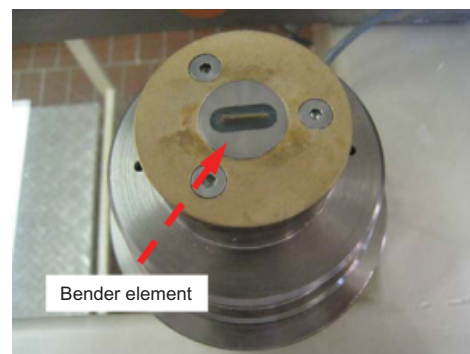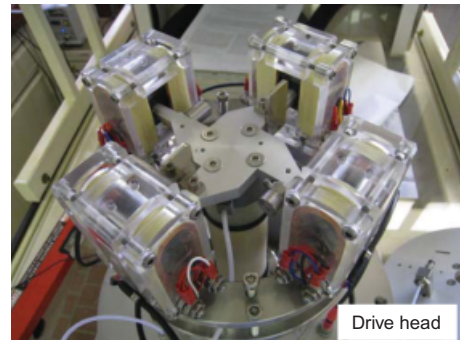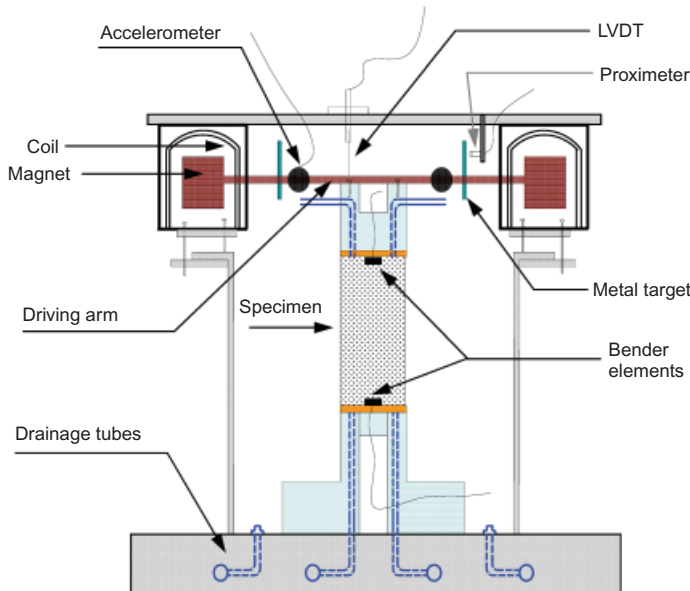LVDT: linear variable deformation transducer

Fig. 3. Close-up views of apparatus (not to scale)

Test material and sample preparation

Three types of uniformly graded glass beads were prepared for the experiment. Fig. 4 shows their size distribution curves, along with a scanning electron microscopy (SEM) photograph showing the shape of the particles. Glass beads of type A, denoted GB-A, were the coarsest, with a mean particle size (D_{50}) of 1·750 mm; glass beads of type D (GB-D) were the finest, with a D_{50} of 0·195 mm; and glass beads of type B (GB-B) with a D_{50} of 0·920 mm were in between (Table 1). The range of particle size was reasonably wide to cover the sizes of fine to coarse sand, and all three types of glass beads shared a similar gradation ($C_u = 1·22–1·25$)
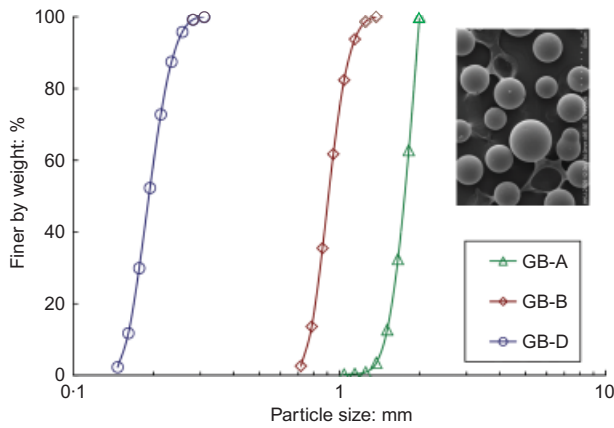
Fig. 4. Particle-size distribution curves of glass beads used in experiments

Table 1. Physical properties of glass beads tested

Glass bead	G_s	D_{10}: mm	D_{50}: mm	D_{60}: mm	C_u
GB-A	2·462	1·48	1·750	1·81	1·22
GB-B	2·462	0·77	0·920	0·94	1·22
GB-D	2·462	0·16	0·195	0·20	1·25

such that the influence of uniformity was isolated. The uniformity of the glass beads is comparable to that of Toyoura sand (1·392), tested by Yang & Gu (2010) using the same apparatus.

Industrially made glass beads may not be perfectly spherical. This defect in shape regularity was observed in all three types of glass beads. From a statistical point of view, however, it can be assumed that these glass beads have a similar roundness and surface roughness, and the potential effect of shape defect or the effect of difference in surface roughness on test results is minor.

Prior to the stiffness measurements, the glass beads were oven-dried and then cooled in sealed containers to remove the potential influence of moisture on the particle surface. All specimens in the tests were prepared using the dry tamping method in five layers. The method involved pouring the material using a funnel without falling height and then performing compaction using a tamper. Note that in the preparation of specimens at the loose state, no significant tamping was used. To stand the specimens and support the weight of the drive arm of the resonant column, a suction of 25 kPa was applied to the specimens. The cell pressure was then increased and the suction was decreased simultaneously to keep a constant isotropic effective confining stress of 25 kPa, which was taken as the initial stress level of the specimens.

Test series
For each type of glass beads a set of specimens were prepared in different initial packing states: loose ($e = 0.595–0.623$), medium-dense ($e = 0.575–0.587$) and dense ($e = 0.558–0.567$) states. For each packing density, the BE and RC tests were conducted at the confining stresses of 50, 100, 200 and 400 kPa in sequence. In bringing the specimens to a specific stress level, each specimen was first consolidated for 15 min at this stress level, and the corresponding deformation was measured by the internal high-resolution linear variable differential transducer (LVDT) (the reading of the LVDT usually became stable within the time allowed); then the BE test was performed under a range of excitation

frequencies. Following the BE test, the RC test was then performed on the same specimen for the purpose of comparison of the stiffness measurements. Table 2 summarises the test series.

BENDER ELEMENT MEASUREMENTS
Despite the increasing popularity of BE tests, considerable uncertainty remains in signal interpretation, and thus in the estimated shear stiffness. Clayton (2011) showed a good example of large scatter in shear wave velocities estimated from a single BE test on a specimen of natural clay, commenting that previous estimates of the accuracy of BE measurements have been optimistic. This opinion is supported by the largely scattered results of the international parallel BE tests on uniform Toyoura sand (Yamashita *et al.*, 2009). These observations, together with the contradictory results in the literature for stiffness variation with particle size, underscore the need for careful examination of BE tests, particularly for granular material, in which wave propagation is complex owing to its particulate nature. Here, efforts are made to clarify several issues that have not yet been extensively studied but are closely related to the reliability of BE measurements: (a) the characteristics of received signals in both the time and frequency domains over a wide range of excitation frequencies and wavelengths; (b) how changes of particle size alter the characteristics of received signals; and (c) the performance of different interpretation methods under a variety of combinations of test conditions (i.e. grain size, excitation frequency and confining stress).

Effect of frequency on waveforms
Figure 5 shows the waveforms generated in a specimen of coarse glass beads (GB-A, $D_{50} = 1.750$ mm) by one cycle of sinusoidal signal at different excitation frequencies. The specimen was at an isotropic confining stress of 100 kPa and a void ratio of 0·584. The excitation frequencies covered a wide range, varying from 1 kHz to as high as 40 kHz, thus allowing a systematic examination of the frequency effect. The dashed line indicates the travel time of the shear wave in the specimen, deduced from the shear wave velocity determined by the RC test. By comparison, the upward triangle indicates the first arrival of the shear wave based on the waveform at the frequency of 10 kHz. Evidently, as the excitation frequency increases, the received signal tends to contain more high-frequency components. At very high excitation frequencies (20 kHz and 40 kHz), the waveforms become quite similar in shape. In addition, the initial signal component with negative polarity preceding the arrival of the major components – marked by a downward triangle and representing the near-field effect – appears to be strongest at the excitation frequency of 1 kHz, and tends to fade as the excitation frequency increases.

Similar observations have been obtained on a medium-coarse specimen (GB-B, $D_{50} = 0.920$ mm), which was also at an isotropic confinement of 100 kPa and a void ratio of 0·585, and was also excited by a sinusoidal input of varying frequencies (Fig. 6). Compared with the waveforms shown in Fig. 5, the received signal at each corresponding frequency contains components of higher frequencies, implying that a change in particle size can affect the frequency content of the received signal. This feature becomes more evident in Fig. 7, where the waveforms in a fine specimen (GB-D, $D_{50} = 0.195$ mm) under various excitation frequencies are shown. Also, it is to be noted that when the grain size reduces from 1·750 mm to 0·195 mm, the initial component with negative polarity tends to fade as well.

Table 2. Summary of test series

Test series	Material	State 0 (e, σ')	State 1 (e, σ')	State 2 (e, σ')	State 3 (e, σ')	State 4 (e, σ')	Note
I-1	GB-A	(0·560, 25)	(0·560, 50)	(0·560, 100)	(0·558, 200)	(0·557, 400)	Dense
		(0·566, 25)	(0·566, 50)	(0·565, 100)	(0·564, 200)	(0·563, 400)	
		(0·559, 25)	(0·559, 50)	(0·558, 100)	(0·557, 200)	(0·556, 400)	
		(0·558, 25)	(0·558, 50)	(0·557, 100)	(0·556, 200)	(0·555, 400)	
		(0·558, 25)	(0·558, 50)	(0·557, 100)	(0·556, 200)	(0·554, 400)	
I-2		(0·583,25)	(0·583, 50)	(0·582, 100)	(0·581, 200)	(0·579, 400)	Medium
		(0·585, 25)	(0·585, 50)	(0·584, 100)	(0·583, 200)	(0·581, 400)	
		(0·582, 25)	(0·582, 50)	(0·581, 100)	(0·580, 200)	(0·578, 400)	
I-3		(0·603, 25)	(0·603, 50)	(0·602, 100)	(0·601, 200)	(0·600, 400)	Loose
		(0·598, 25)	(0·598, 50)	(0·597, 100)	(0·596, 200)	(0·594, 400)	
		(0·595, 25)	(0·595, 50)	(0·594, 100)	(0·593, 200)	(0·591, 400)	
II-1	GB-B	(0·561, 25)	(0·561, 50)	(0·560, 100)	(0·559, 200)	(0·558, 400)	Dense
		(0·562, 25)	(0·562, 50)	(0·561, 100)	(0·560, 200)	(0·558, 400)	
		(0·567, 25)	(0·567, 50)	(0·566, 100)	(0·565, 200)	(0·563, 400)	
		(0·566, 25)	(0·566, 50)	(0·565, 100)	(0·564, 200)	(0·562, 400)	
		(0·561, 25)	(0·561, 50)	(0·560, 100)	(0·559, 200)	(0·557, 400)	
II-2		(0·584, 25)	(0·583, 50)	(0·583, 100)	(0·582, 200)	(0·580, 400)	Medium
		(0·586, 25)	(0·586, 50)	(0·585, 100)	(0·584, 200)	(0·582, 400)	
II-3		(0·603, 25)	(0·603, 50)	(0·602, 100)	(0·601, 200)	(0·599, 400)	Loose
		(0·601, 25)	(0·600, 50)	(0·600, 100)	(0·598, 200)	(0·597, 400)	
		(0·596, 25)	(0·596, 50)	(0·595, 100)	(0·594, 200)	(0·592, 400)	
		(0·598, 25)	(0·598, 50)	(0·597, 100)	(0·596, 200)	(0·594, 400)	
		(0·601, 25)	(0·601, 50)	(0·600, 100)	(0·598, 200)	(0·596, 400)	
III-1	GB-D	(0·564, 25)	(0·563, 50)	(0·563, 100)	(0·561, 200)	(0·560, 400)	Dense
		(0·564, 25)	(0·563, 50)	(0·563, 100)	(0·562, 200)	(0·560, 400)	
III-2		(0·587, 25)	(0·586, 50)	(0·585, 100)	(0·584, 200)	(0·582, 400)	Medium
		(0·585, 25)	(0·584, 50)	(0·583, 100)	(0·582, 200)	(0·580, 400)	
		(0·584, 25)	(0·584, 50)	(0·583, 100)	(0·582, 200)	(0·579, 400)	
		(0·575, 25)	(0·575, 50)	(0·574, 100)	(0·573, 200)	(0·571, 400)	
III-3		(0·603, 25)	(0·602, 50)	(0·601, 100)	(0·600, 200)	(0·598, 400)	Loose
		(0·601, 25)	(0·601, 50)	(0·600, 100)	(0·599, 200)	(0·596, 400)	
		(0·616, 25)	(0·615, 50)	(0·615, 100)	(0·614, 200)	(0·612, 400)	
		(0·623, 25)	(0·623, 50)	(0·622, 100)	(0·621, 200)	(0·619, 400)	

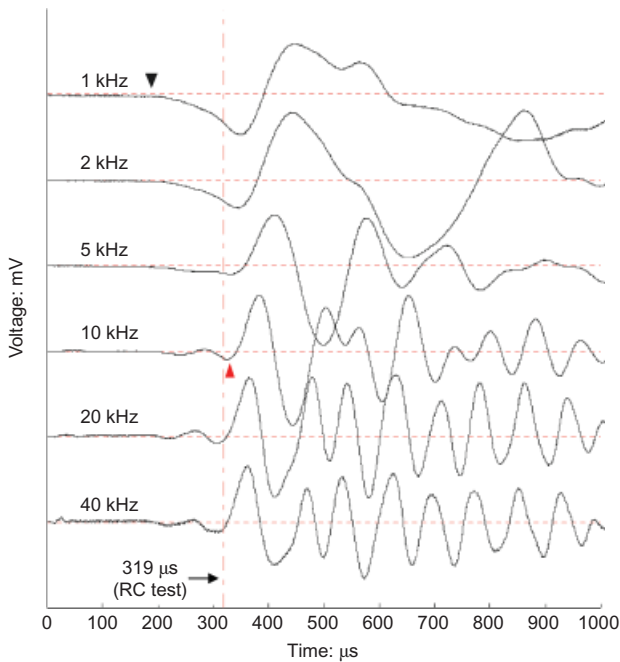Note: e = void ratio; σ' = effective confining stress (in kPa); state 0 = initial state.

Fig. 5. Shear wave signals in glass beads GB-A ($D_{50} = 1.750$ mm) at various excitation frequencies (sinusoidal input, $\sigma' = 100$ kPa; $e = 0.584$)
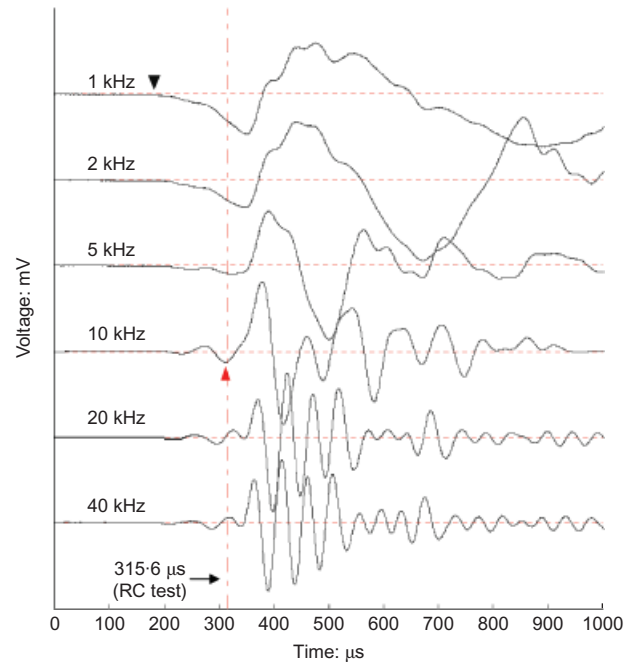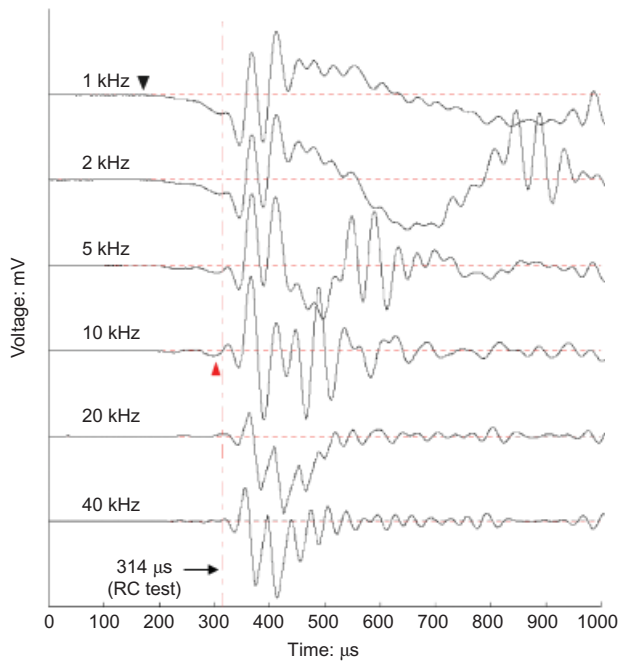

Fig. 6. Shear wave signals in glass beads GB-B ($D_{50} = 0.920$ mm) at various excitation frequencies (sinusoidal input, $\sigma' = 100$ kPa; $e = 0.585$)
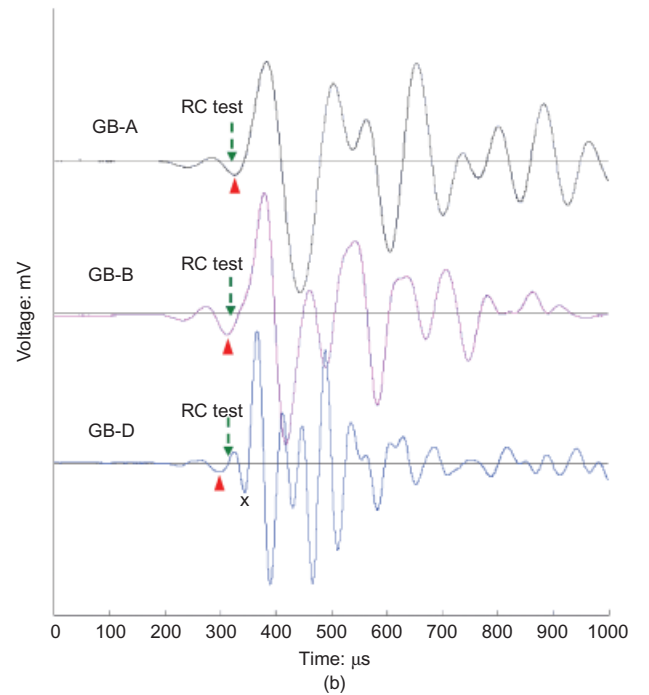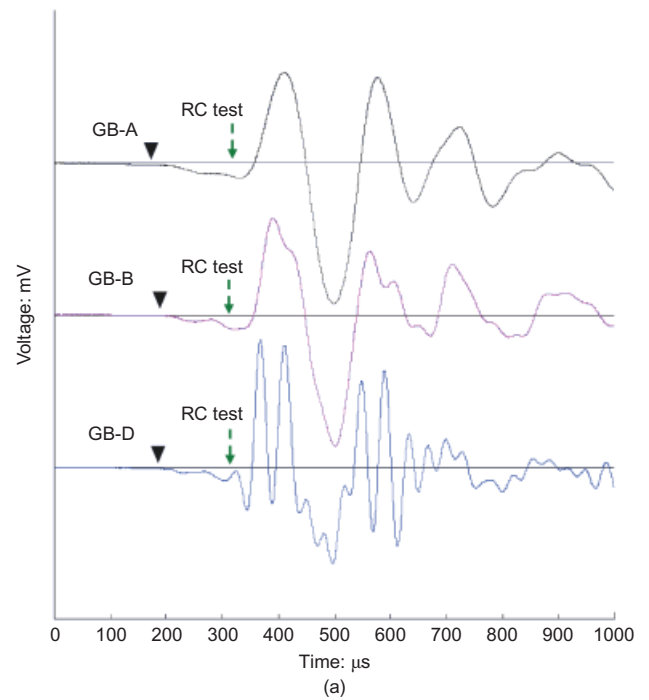
Fig. 7. Shear wave signals in glass beads GB-D ($D_{50} = 0\cdot195$ mm) at various excitation frequencies (sinusoidal input, $\sigma' = 100$ kPa; $e = 0\cdot583$)

Effect of particle size on waveforms

To allow a better identification of the importance of particle size in modifying waveforms, Fig. 8 compares the waveforms generated in the three specimens under otherwise similar conditions. The waveforms at the excitation frequency of 5 kHz are compared in Fig. 8(a), and another three waveforms at the excitation frequency of 10 kHz are compared in Fig. 8(b). In either case of excitation frequency, a decrease in grain size can introduce high-frequency components to the output signal. The waveforms in the finest specimen GB-D, at either 5 kHz or 10 kHz, exhibit a first peak with an amplitude that is much less than the subsequent largest peak. It is the excursion of this small peak that represents the true arrival of the shear wave (marked by an upward triangle on the waveform for specimen GB-D in Fig. 8(b)). For purposes of comparison, the travel times of the shear waves in the three specimens were deduced from the RC measurements, and are marked by three downward dashed arrows on the corresponding waveforms. It becomes clear that, if the excursion of the largest peak is selected as the arrival of the shear wave (marked by the indicator 'x'), a stiffness value substantially lower than the RC measurement will be yielded.

The existence of a small-amplitude peak preceding the largest peak in the shear wave signal was also reported by Brignoli *et al.* (1996) in pulse tests on uniform Ticino sand ($D_{50} = 0\cdot710$ mm); it was also observed in testing Toyoura sand ($D_{50} = 0\cdot216$ mm) using the same apparatus (Yang & Gu, 2010), as shown in Fig. 9 for comparison. This feature is not evident in the waveforms generated in the coarsest specimen (GB-A; Fig. 5), but for the medium-coarse specimen (GB-B) the feature tends to appear when the excitation frequency is sufficiently high (Fig. 6). It is also found that, for a given excitation frequency, increasing the confining stress to large levels tends to result in the occurrence of the small peak, as shown in Fig. 10 for glass beads GB-B.

The waveforms in Figs 5–8 and the discussion above show the important finding that the effect of particle size is coupled with the effect of frequency in altering the characteristics of waveforms. This is understandable, given the parti-

Fig. 8. Shear wave signals in glass beads of different sizes (sinusoidal input, $\sigma' = 100$ kPa; $e \approx 0\cdot584$): (a) excitation frequency = 5 kHz; (b) excitation frequency = 10 kHz

culate nature of the material. To explore their relation, the fast Fourier transform was conducted for the output signals in Figs 5–7, and the predominant frequency was identified for each signal. Fig. 11 shows this predominant frequency, denoted as f_{out}, as a function of the excitation frequency (f_{in}) for the three specimens, together with the trend lines. There are several features in Fig. 11 that are worth noting. First, for either coarse or fine specimens, the predominant frequency tends to increase with excitation frequency in an approximately linear manner in a low-frequency range, and then tends to approach a limiting value at high excitation frequencies. In this respect, a threshold frequency marking the transition can be identified. Second, this threshold frequency appears to depend on particle size, in that it takes larger
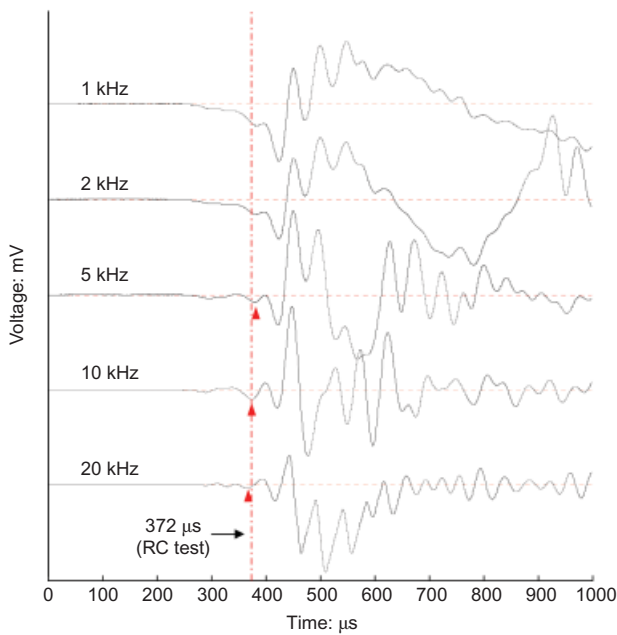
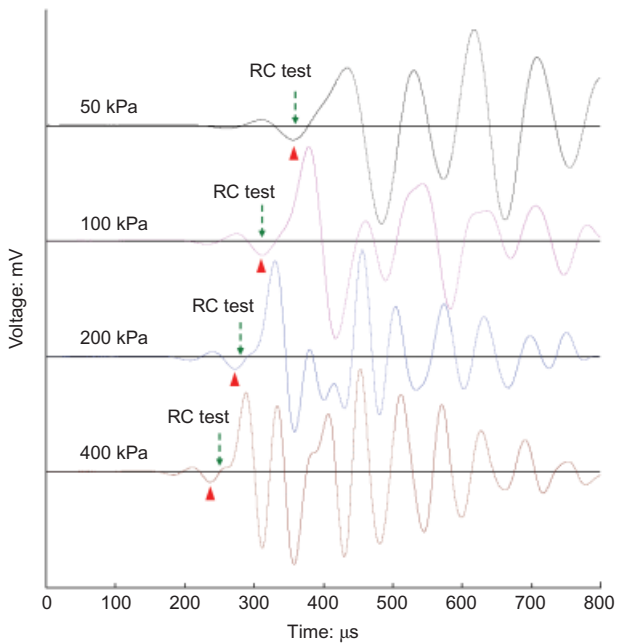Fig. 9. Shear wave signals in dry Toyoura sand at various excitation frequencies ($\sigma' = 100$ kPa; $e = 0.798$)

Fig. 11. Output signal frequency against input signal frequency

Fig. 10. Shear wave signals in glass beads GB-B at various confining stresses (sinusoidal input, $e \approx 0.585$)

the shear wave signal generated in a granular sample, even with a simple sinusoidal input, can be very complicated. Its characteristics depend on both excitation frequency and particle size, and these factors are interrelated. With regard to shear stiffness measurement, the important implication is that diverse or even contradictory results may be yielded on the shear wave velocity (V_s) or the small-strain stiffness (G_0) if these factors are not properly taken into account in data interpretation; this will be elaborated in more detail in the following section.

Evaluation of various interpretation methods

The largest uncertainty and difficulty with BE tests lie in determination of the travel time of the shear wave (Jovicic *et al.*, 1996; Lee & Santamarina, 2005; Yamashita *et al.*, 2009). The commonly used approaches, as documented in Yamashita *et al.* (2009), are generally simplistic, and do not well recognise that the boundary conditions imposed on the specimen can lead to considerable divergence from the simplified solutions. One of the common approaches is known as the start-to-start method and another is the peak-to-peak method, both working in the time domain. The idea of the start-to-start method is to find the first arrival of the shear wave by visual inspection of the received signal. A number of characteristic points have been proposed in the literature as indicators for the first arrival of the shear wave. A systematic examination of differences in the estimated shear stiffness using these points has been conducted for both fine and coarse specimens, with particular attention paid to the size effect. To facilitate discussion, a typical waveform is shown in Fig. 12, with all possible characteristic points marked as the first arrival of the shear wave, including the first inflection S1, the troughs S2 and S4, and the zero intercepts S3 and S5.

The peak-to-peak method applies typically to a sinusoidal input in which the travel time is defined as the difference between the peak of the input signal and that of the output signal. As the received signal usually contains multiple peaks rather than a single peak, a common practice is to take the largest peak to estimate the travel time (P2 in Fig. 12). However, as will be further explored later, in many cases this largest peak does not offer a reasonable reference for determining the travel time of the shear wave; as an alternative, a smaller peak preceding the maximum one (P1 in Fig. 12) is also used for comparison purposes.

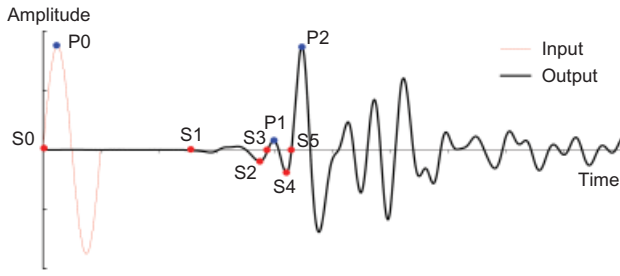To overcome the subjectivity and uncertainty involved in

values for fine specimens or smaller values for coarse specimens. For example, for specimen GB-A the threshold frequency is around 16 kHz, whereas it is above 20 kHz for specimen GB-D. Third, the predominant frequency does not appear to be sensitive to particle size in the range of low excitation frequency (say, below 5 kHz); however, as the excitation frequency is further increased, it tends to become larger for fine specimens than for coarse specimens. Moreover, the limiting value of the predominant frequency at high excitation frequencies seems to increase with decreasing particle size. The interesting features described above are based on the experiments conducted on uniform glass beads; further validation using laboratory tests on different granular materials would be of benefit.

The experimental data described above offer evidence that

Fig. 15. Shear stiffness values estimated using various interpretation methods as a function of ratio between travel distance and wavelength ($\sigma' = 100$ kPa): (a) GB-A, $e = 0.584$; (b) GB-B, $e = 0.585$; (c) GB-D, $e = 0.583$

method using point S2 seems to work well for the fine specimen GB-D, whereas the start-to-start method using point S4 seems to work well for the coarse specimens GB-A and GB-B, for which point S2 appears to merge with point S4 (see Fig. 8(b)).

(c) The performance of the cross-correlation method using either CC-1 or CC-2 is improved in this optimal R_d^{in} range, but the method still provides G_0 values that are more than 20% lower than the corresponding RC measurements.

Bearing in mind the coupled effects of excitation frequency and particle size, a new index is introduced as the ratio between wavelength (λ) and mean particle size (D_{50}), and variations of the normalised G_0 values with this index are examined in Fig. 16. To facilitate comparison, the data shown in Fig. 16(a) were all generated using the start-to-start method, the data in Fig. 16(b) were generated using the peak-to-peak method, and Fig. 16(c) was produced using the cross-correlation method. Note that the wavelength was

calculated using the frequency of the input sinusoidal signal and the RC reference value for shear wave velocity.

The three plots in Fig. 16 offer several important findings.

(a) The start-to-start method using either point S5 or S4 tends to give G_0 values that decrease as the λ/D_{50} ratio increases: that is, for a given excitation frequency, the shear stiffness will decrease with decreasing particle size.

(b) The peak-to-peak method using P0–P2 (i.e. the largest peak) tends to give G_0 values that increase as the λ/D_{50} ratio increases; this means that, for a given excitation frequency, the shear stiffness increases with decreasing particle size.

(c) The cross-correlation method also produces G_0 values that increase with increasing λ/D_{50} ratio, either due to a decrease in particle size or to a reduction of excitation frequency. Also, the start-to-start method using point S2 is able to consistently provide reasonable G_0 values over a wide range of λ/D_{50} ratios (20–1000). These G_0 values are slightly greater than the RC benchmark values, and
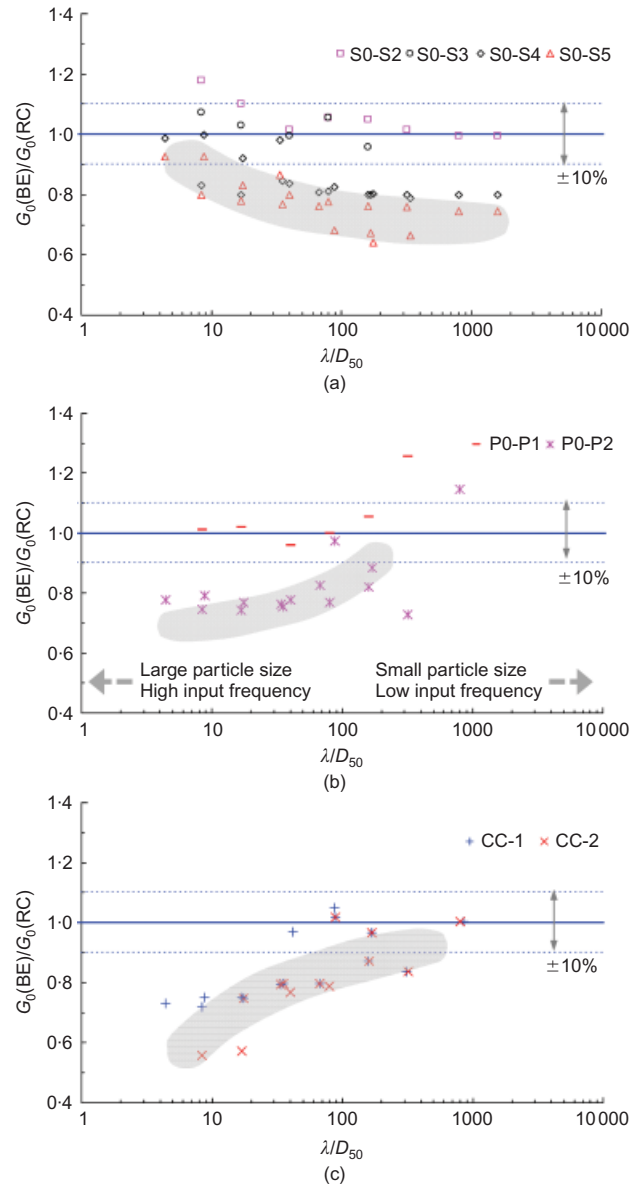
Fig. 16. Shear stiffness values estimated using various interpretation methods as a function of ratio between wavelength and particle size ($\sigma' = 100$ kPa; $e \approx 0.584$): (a) start-to-start method; (b) peak-to-peak method; (c) cross-correlation method

exhibit a tendency to decrease with λ/D_{50} ratio, but the variation is approximately less than 10%.

Based on a systematic examination of the characteristics of waveforms, and taking the RC measurements as a reference, the following strategies are recommended for conducting and interpreting BE tests for stiffness measurement.

(a) A range of excitation frequencies covering the threshold frequency should be used, and the waveforms at various frequencies should be examined as a whole.

(b) The excitation frequencies should be selected such that the ratio of travel distance and wavelength is between 2 and 4 (higher R_d^{in} values do not seem to help reduce the uncertainty).

(c) The start-to-start method using point S2 is recommended; for coarse materials where point S2 is not clear, point S4 is a reasonable alternative.

COMPARISONS OF BE AND RC MEASUREMENTS

A large number of BE and RC tests have been performed over a range of confining stresses and void ratios, and thereby offer an excellent opportunity to compare the stiffness values from the two methods. In doing so, the BE and RC measurements of the small-strain stiffness are shown against confining stress in Figs 17(a), 17(b) and 17(c) for specimens GB-A, GB-B and GB-D, respectively. It is evident that G_0 values estimated from both the RC and BE tests show an increase with the confining stress. As indicated by the trend lines for the upper and lower bounds, the stress dependence can be well represented by a power law, with the exponent being about 0·4. The data also indicate that at a given confining stress the G_0 value decreases with increasing void ratio. Using the empirical formula given in equation (1) to account for the effects of confining stress and void ratio, the two parameters A and n have been determined for the RC and BE measurements, respectively (see Table 3). For the purpose of comparison, values of the two parameters determined using test data for Toyoura sand (Yang & Gu, 2010) are also included.

It is of interest to note from Fig. 17 and Table 3 that for fine granular materials (GB-D and Toyoura sand) the BE measurements are apparently greater than the RC measurements, whereas for coarse granular materials (GB-A) the two methods give G_0 values that are consistent overall. The results for the medium-coarse glass beads (GB-B) appear to be in between, with the BE measurements being slightly greater than the RC measurements. This marked feature can be found in an alternative way, as shown by Fig. 18, where the BE measurements of G_0 are plotted against the RC measurements. For both the fine and coarse specimens, the difference between the BE and RC measurements is approximately within 10%, meaning that the effect of testing method is practically negligible.

Possible reasons for the finding that BE measurements of stiffness are larger than the corresponding ones from RC tests for fine and medium-coarse granular may be that: (a) the overall strain level involved in BE tests is somehow lower than that involved in RC tests; and (b) the RC test measures the overall stiffness of the specimen, whereas the BE test measures the central part of the specimen between the transmitter and receiver (Fig. 19), which tends to be stiffer than the whole specimen in the case of fine and medium-coarse granulates. Further work to explore the reasons behind this interesting observation would be of interest.

Figure 20 shows variations of stiffness values, determined by the BE and RC tests, with particle size at the dense, medium-dense and loose states. An alternative view of the
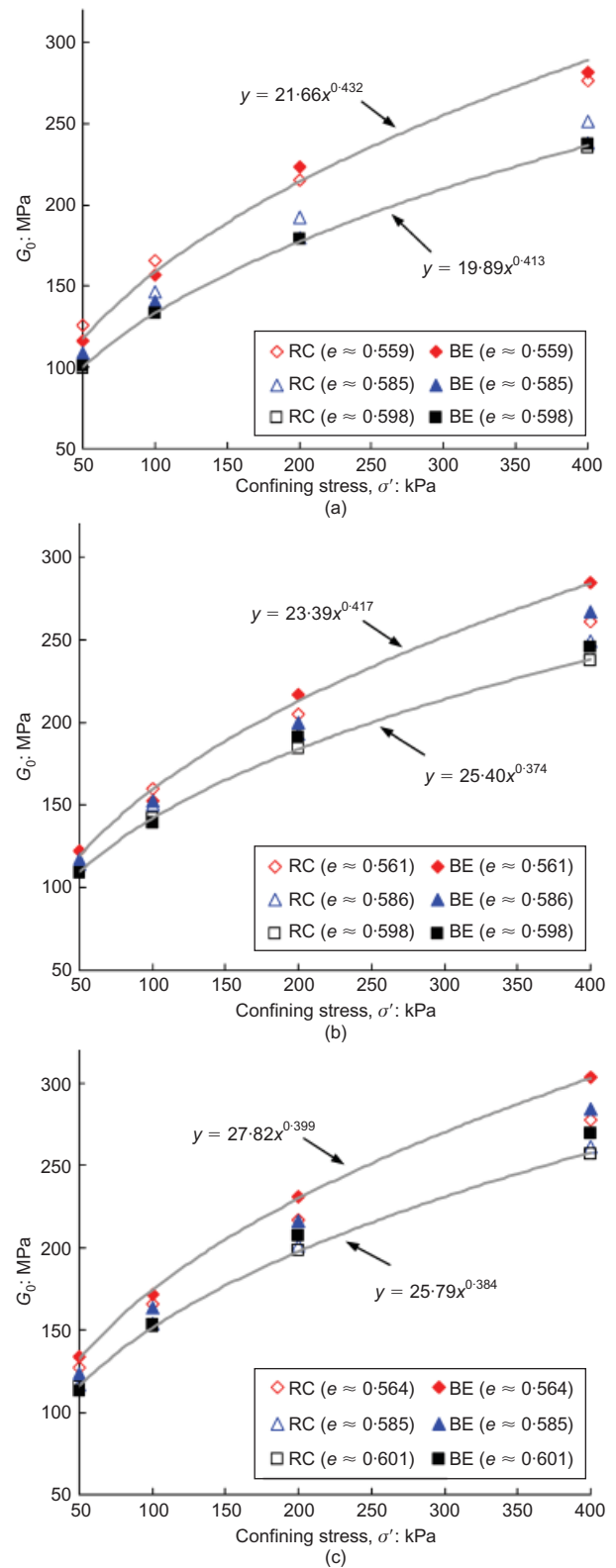
Fig. 17. Shear stiffness as function of confining stress: (a) GB-A, $D_{50} = 1.750$ mm; (b) GB-B, $D_{50} = 0.920$ mm; (c) GB-D, $D_{50} = 0.195$ mm

results is given in Fig. 21, where the BE measurements normalised by the corresponding RC measurements are shown as a function of particle size. Both BE and RC measurements show a trend that G_0 values decrease slightly with mean particle size D_{50}, particularly for specimens at the loose state. However, given that the variations are approximately within 10%, and given the uncertainty in-

Table 3. Best-fit parameters for shear stiffness measurements

Material	Test method	Parameters		
		$F(e)$	A	n
GB-A	G_0 (BE)	$F(e) = \dfrac{(2 \cdot 17 - e)^2}{1 + e}$	88·91	0·39
	G_0 (RC)		91·22	0·40
GB-B	G_0 (BE)		90·73	0·40
	G_0 (RC)		87·80	0·40
GB-D	G_0 (BE)		97·12	0·41
	G_0 (RC)		92·79	0·39
Toyoura sand	G_0 (BE)		95·10	0·41
	G_0 (RC)		92·50	0·41

Note: A and n are the two parameters in equation (1).

volved in the experiments and data interpretations, this modest size effect may, to a first approximation, be neglected: that is, the shear stiffness is assumed to be size independent for the range of particle sizes examined.

MICROMECHANICAL CONSIDERATIONS

From the micromechanical point of view, the small-strain shear stiffness of an assembly of particles should be closely related to the properties of discrete particles that interact with each other. To make this point, a grain-scale analysis is presented here. Note that this analysis is not aimed to explain the diverse features of the waveforms observed in the BE tests.

Consider a simple cubic array of identical spherical particles with dimension l, and subjected to an isotropic stress σ', as shown in Fig. 22. The number of spheres in each dimension is m, and the sphere is characterised by its radius R, Young's modulus E_g, and Poisson's ratio ν_g or shear modulus G_g $(= E_g/2(1 + \nu_g))$. Assuming that the Hertz–Mindlin contact law (Mindlin & Deresiewicz, 1953; Duffy & Mindlin, 1957) applies, the normal stiffness between two spheres that are in contact can be given as

$$k_n^t = \frac{dN}{d\varpi} = \frac{3}{4} \left(\frac{R^{1/2}}{\zeta} \right)^{2/3} N^{1/3} \qquad (4)$$

$$\zeta = \frac{3(1 - \nu_g^2)}{4 E_g} \qquad (5)$$

where N is the normal contact force between the two spheres, and ϖ is the normal displacement. Similarly, the shear contact stiffness of the two spheres can be given by

$$k_s^t = \frac{dT}{d\delta} = \left(\frac{4 G_g}{2 - \nu_g} \right) (\zeta R N)^{1/3} \left(1 - \frac{T}{\mu N} \right)^{1/3} \qquad (6)$$

where T is the shear contact force, δ is the tangential displacement between the spheres under shear, and μ is the friction coefficient between the two spheres. Note that for the cubic array the normal contact force N can be calculated by

$$N = 4\sigma' R^2 \qquad (7)$$

The normal contact stiffness and the tangential contact stiffness can be further expressed as

$$k_n^t = A_1 (\sigma')^{1/3} R \qquad (8)$$

$$k_s^t = A_2 (\sigma')^{1/3} R \left(1 - \frac{T}{\mu N} \right)^{1/3} \qquad (9)$$

where

$$A_1 = 3 \left[\frac{3(1 - \nu_g^2)}{E_g} \right]^{-2/3} \qquad (10)$$

$$A_2 = \frac{2}{2 - \nu_g} \left[12 G_g^2 (1 - \nu_g) \right]^{1/3} \qquad (11)$$

To determine the shear stiffness of the cubic array, a small shear stress increment $\Delta\tau$ is applied to the array, and the corresponding shear strain is then calculated from

$$\begin{aligned} \Delta\gamma &= \frac{4m}{l} \frac{\Delta\tau R^2}{k_s^t} \\ &= \frac{4m}{l} \frac{\Delta\tau R^2}{A_2 R (\sigma')^{1/3} [1 - (T/\mu N)]^{1/3}} \end{aligned} \qquad (12)$$

The shear stiffness of the simple cubic array can then be given by

$$G_0 = \frac{\Delta\tau}{\Delta\gamma} = \frac{1}{2} A_2 (\sigma')^{1/3} \left(1 - \frac{T}{\mu N} \right)^{1/3} \qquad (13)$$

It is evident from equation (13) that the shear stiffness of the array is independent of the radius of the sphere. In other words, the particle size has no effect on the stiffness of the array.

SUMMARY AND CONCLUSIONS

This paper has identified and addressed two fundamental questions on the small-strain shear stiffness of granular material: particle size dependence and the effect of testing method. For three uniform types of glass beads with mean grain sizes varying from 0·195 mm to 1·750 mm, series of BE and RC tests have been performed for a range of confining stresses and void ratios. Micromechanical modelling has also been conducted to offer an understanding from the grain scale. The key findings from the laboratory experiments are summarised as follows.

(a) The BE measurements of small-strain stiffness are comparable to the RC measurements, with differences being less than about 10%. The BE measurements for the fine glass beads tend to be consistently larger than the resonant column measurements, especially at high confining stress levels, whereas this feature becomes less evident for the medium-coarse glass beads, and eventually diminishes for the coarse glass beads.

(b) The BE and RC tests both show a trend that the small-strain stiffness (G_0) decreases slightly with mean particle

(a)

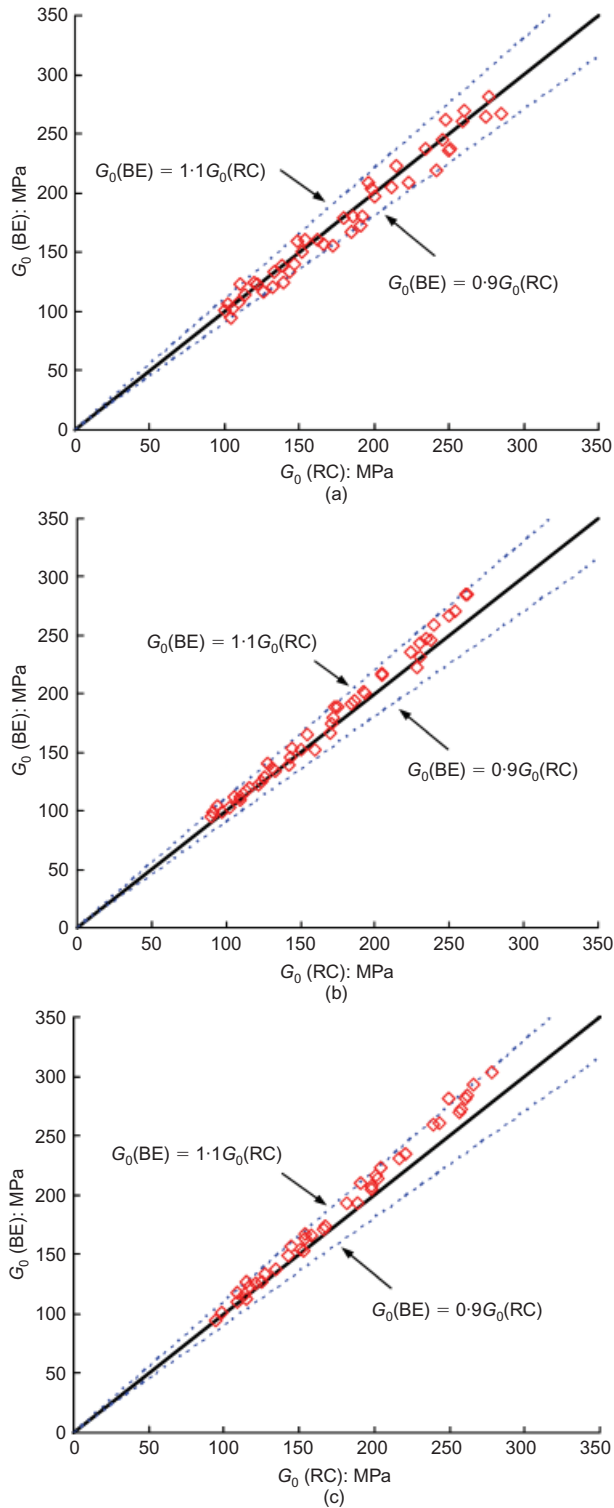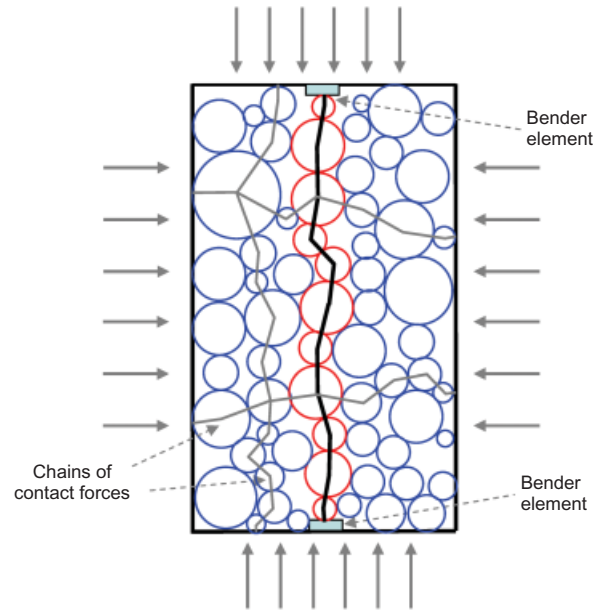(b)

(c)

Fig. 18. Comparisons of shear stiffness measurements from BE and RC tests: (a) GB-A, $D_{50} = 1 \cdot 750$ mm; (b) GB-B, $D_{50} = 0 \cdot 920$ mm; (c) GB-D, $D_{50} = 0 \cdot 195$ mm

Fig. 19. Schematic illustration of wave paths and force chains in bender element tests

size (D_{50}), particularly for glass beads at the loose state. Given that the variations in the measured stiffness values are generally small, and given the uncertainty in the laboratory experiments, it may be practically assumed that small-strain stiffness is size independent. This result is confirmed by the micromechanics-based analysis using the Hertz–Mindlin contact law.

(c) The waveforms generated in a granular specimen in BE tests are complex, depending largely on the excitation frequency, the size of particles, and the confining stress level. The predominant frequency of the output signal tends to increase with excitation frequency, and then approach a limiting value at high frequencies. A threshold frequency marking this transition seems to exist, and both the threshold frequency and the limiting frequency show a tendency to increase with decreasing particle size.

(d) Under otherwise similar conditions, a decrease in particle size can result in high-frequency components in the output signal. The waveforms generated in fine granular specimens display a small-amplitude peak preceding the largest peak, and this feature tends to be enhanced at high frequencies and at large confining stresses. It is the excursion of the small peak rather than the largest peak that represents the true arrival of the shear wave.

(e) The conventional start-to-start method (using either point S5 or S4) tends to yield low stiffness values that decrease as the λ/D_{50} ratio increases, meaning that the stiffness decreases with decreasing particle size for a given excitation frequency. The conventional peak-to-peak method (using point P2) and the cross-correlation method also give low stiffness values that, however, tend to increase as the λ/D_{50} ratio increases, meaning that for a given excitation frequency the stiffness increases with decreasing particle size.

(f) The degree of scatter in stiffness measurements due to different interpretation methods for BE tests appears to depend on the travel distance-to-wavelength ratio (R_d^{in}). For R_d^{in} values ranging from 2 to 4, the scatter seems to be the smallest; higher R_d^{in} values do not seem to help reduce uncertainty or improve accuracy. In this optimal range of R_d^{in} values the start-to-start method using point S2 works well for fine granular material, whereas the start-to-start method using point S4 works well for coarse specimens in which point S2 appears to merge with point S4.
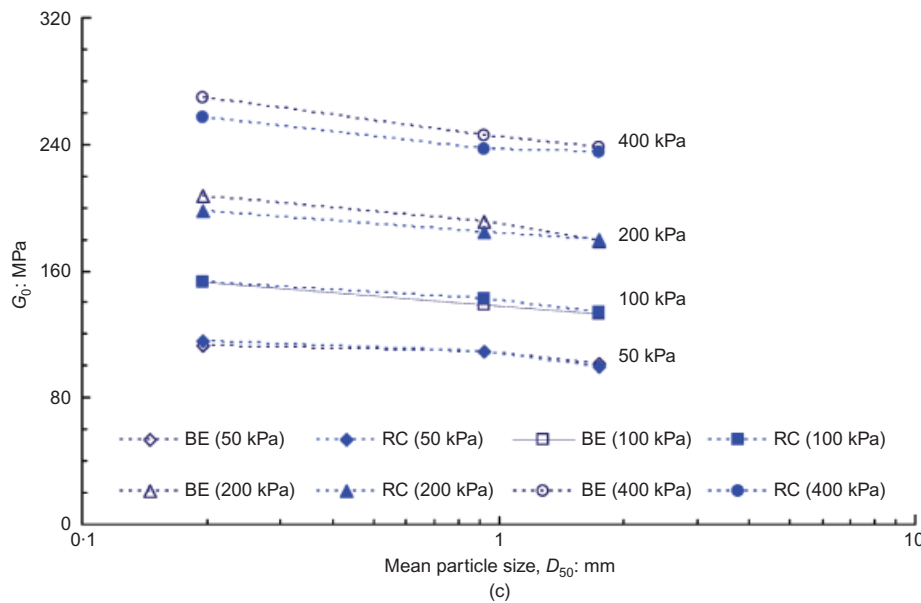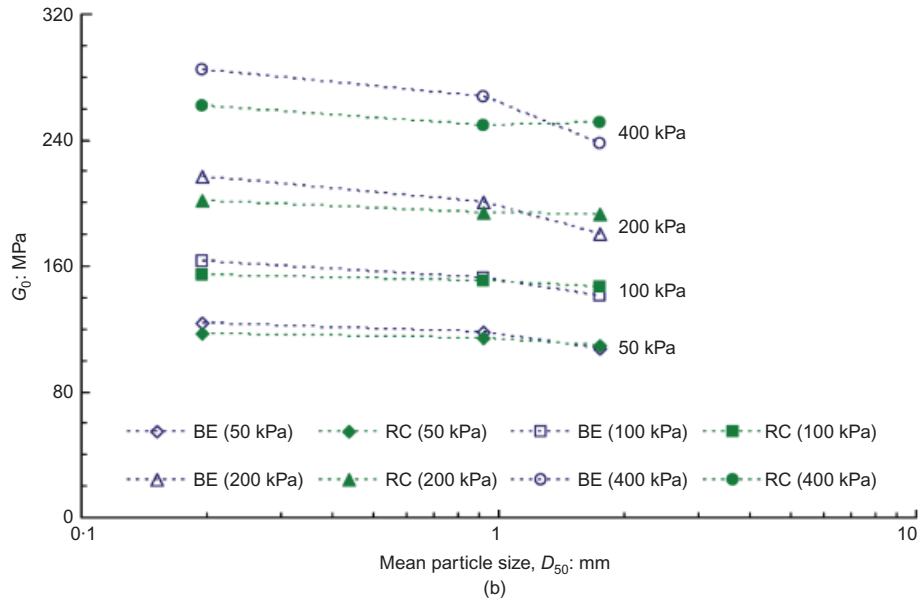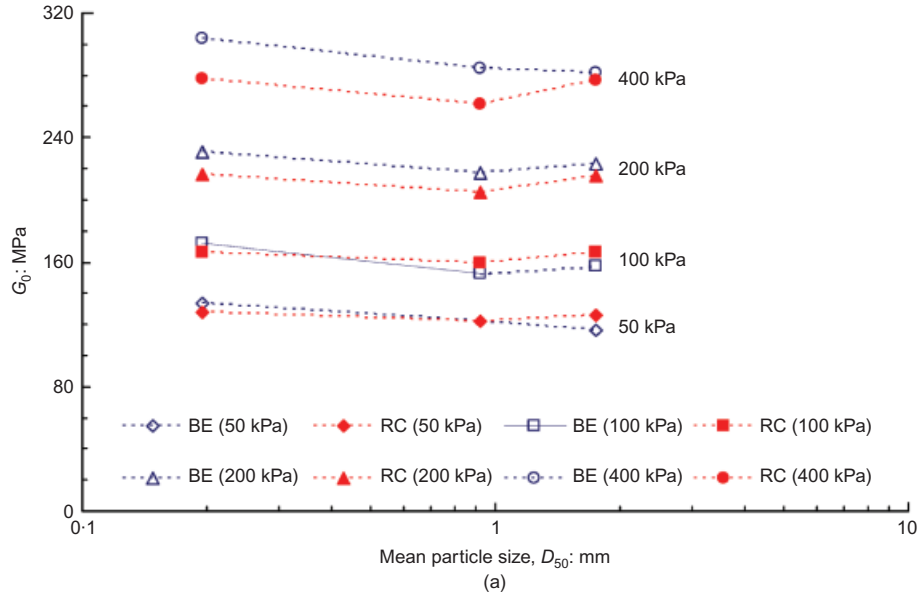
Fig. 20. **Variation of shear stiffness with particle size: (a) dense state; (b) medium-dense state; (c) loose state**
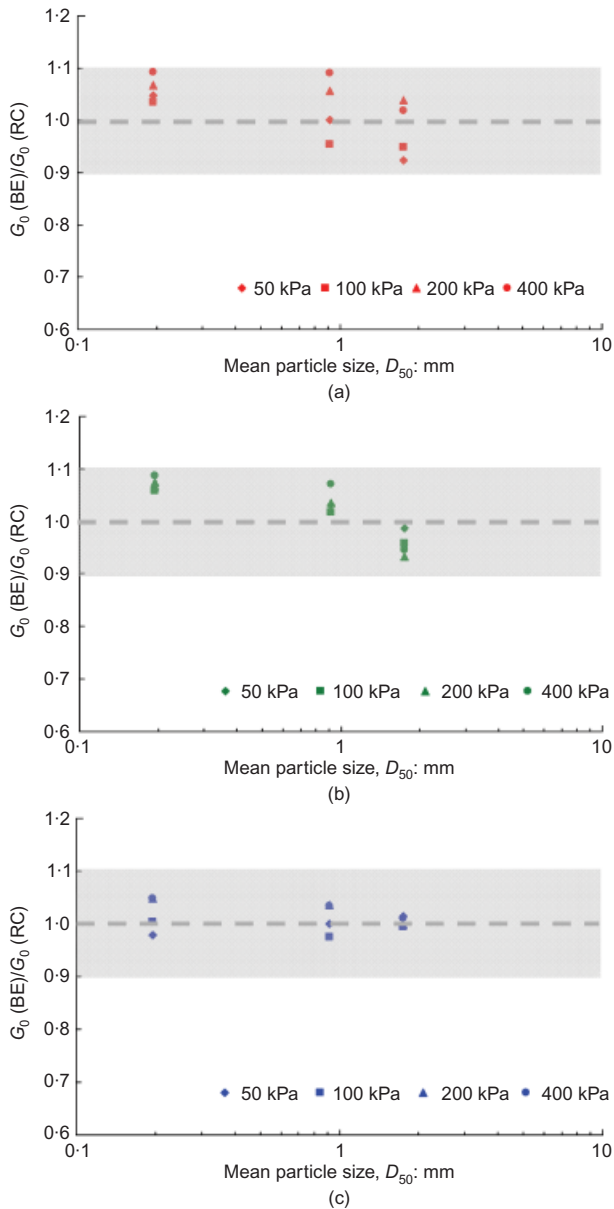
Fig. 21. Variation of shear stiffness ratio with particle size: (a) dense state; (b) medium-dense state; (c) loose state
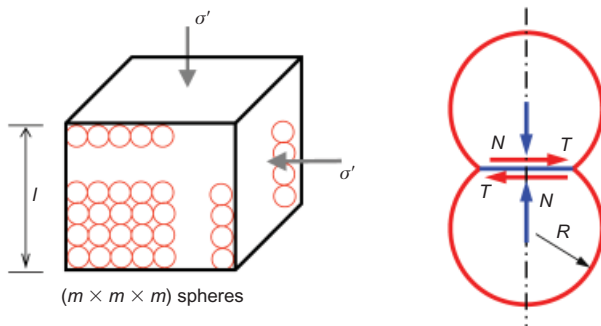

Fig. 22. A cubic array of spheres: Hertz–Mindlin contact model

NOTATION

A	parameter in equation (1)
A_1, A_2	constants in equations (8) and (9)
C_u	coefficient of uniformity
D_{10}	particle size that 10% weight of soil are smaller than
D_{50}	mean particle size
D_{60}	particle size that 60% weight of soil are smaller than
E_g	Young's modulus of grains
e	void ratio
$F(e)$	void ratio function
f_{in}	frequency of input signal in BE test
f_{out}	predominant frequency of output signal in BE test
G_g	shear modulus of grains
G_0 (or G_{max})	soil small-strain shear modulus
k_n^t	normal contact stiffness
k_s^t	shear contact stiffness
l	length of simple cubic array
L_{tt}	travel distance of shear wave
m	number of spheres in each dimension in simple cubic array
N	normal contact force
n	stress exponent
p_a	reference stress
R	radius of sphere
R_d^{in}	ratio of wave travel distance to wavelength based on input frequency
T	shear contact force
V_s	shear wave velocity
$\Delta\gamma$	shear strain induced by shear stress increment
δ	tangential displacement between spheres under shear
λ	wavelength
μ	friction coefficient between spheres
ν_g	Poisson's ratio of grains
ρ	mass density
σ'	effective confining stress
$\Delta\tau$	shear stress increment
ϖ	normal displacement between spheres under compression

REFERENCES

Bartake, P. P. & Singh, D. N. (2007). Studies on the determination of shear wave velocity in sands. *Geomech. Geoengng* **2**, No. 1, 41–49.

Brignoli, E. G. M., Gotti, M. & Stokoe, K. H. II. (1996). Measurement of shear waves in laboratory specimens by means of piezoelectric transducers. *Geotech. Test. J.* **19**, No. 4, 384–397.

Cho, G., Dodds, J. & Santamarina, J. C. (2006). Particle shape effects on packing density, stiffness and strength: natural and crushed sands. *J. Geotech. Geoenviron. Engng ASCE* **132**, No. 5, 591–602.

Chung, R. M., Yokel, F. Y. & Drnevich, V. P. (1984). Evaluation of dynamic properties of sands by resonant column testing. *Geotech. Test. J.* **7**, No. 2, 60–69.

Clayton, C. R. I. (2011). Stiffness at small strain: research and practice. *Géotechnique* **61**, No. 1, 5–38, http://dx.doi.org/10.1680/geot.2011.61.1.5.

Clayton, C. R. I., Priest, J. A., Bui, M., Zervos, A. & Kim, S. G. (2009). The Stokoe resonant column apparatus: effects of stiffness, mass and specimen fixity. *Géotechnique* **59**, No. 5, 429–437, http://dx.doi.org/10.1680/geot.2007.00096.

Duffy, J. & Mindlin, R. D. (1957). Stress-strain relations and vibrations of a granular medium. *J. Appl. Mech.* **24**, 585–593.

Dyvik, R. & Madshus, C. (1985). Lab measurements of G_{max} using bender element. *Proceedings of the ASCE convention on advances in the art of testing soils under cyclic conditions*, Detroit, MI, pp. 186–196.

Hardin, B. O. & Richart, F. E. (1963). Elastic wave velocities in granular soils. *J. Soil Mech. Found. Engng Div. ASCE* **89**, No. SM1, 39–56.

Iwasaki, T. & Tatsuoka, F. (1977). Effect of grain size and grading on dynamic shear moduli of sand. *Soils Found*. **38**, No. 1, 19–35.

Jovicic, V., Coop, M. R. & Simic, M. (1996). Objective criteria for determination of G_{max} from bender element tests. *Géotechnique* **46**, No. 2, 357–362, http://dx.doi.org/10.1680/geot.1996.46.2.357.

Lee, J. S. & Santamarina, J. C. (2005). Bender elements: perform-

ance and signal interpretation. *J. Geotech. Geoenviron. Engng ASCE* **131**, No. 9, 1063–1070.

Lings, M. L. & Greening, P. D. (2001). A novel bender/extender element for soil testing. *Géotechnique* **51**, No. 8, 713–717, http://dx.doi.org/10.1680/geot.2001.51.8.713.

Lo Presti, D. C. F., Jamiolkowski, M., Pallara, O. & Pedroni, A. C. S. (1997). Shear modulus and damping of soils. *Géotechnique* **47**, No. 3, 603–617, http://dx.doi.org/10.1680/geot.1997.47.3.603.

Mindlin, R. D. & Deresiewicz, H. (1953). Elastic spheres in contact under oblique forces. *J. Appl. Mech. ASME* **20**, 327–344.

Patel, A., Bartake, P. P. & Singh, D. N. (2008). An empirical relationship for determining shear wave velocity in granular materials accounting for grain morphology. *Geotech. Test. J.* **32**, No. 1, 1–10.

Sanchez-Salinero, I., Roesset, J. M. & Stokoe, K. H. II. (1986). *Analytical studies of body wave propagation and attenuation*, Report No. GR-86-15. Austin, TX, USA: University of Texas.

Sharifipour, M., Dano, C. & Hicher, P. Y. (2004). Wave velocities in assemblies of glass beads using bender-extender elements.

Proc. 17th ASCE Conf. Engng Mech. (EM2004), University of Delaware.

Viggiani, G. & Atkinson, J. H. (1995). Interpretation of bender element tests. *Géotechnique* **45**, No. 1, 149–154, http://dx.doi.org/10.1680/geot.1995.45.1.149.

Wichtmann, T. & Triantafyllidis, Th. (2009). Influence of the grain-size distribution curve of quartz sand on the small strain shear modulus G_{max}. *J. Geotech. Geoenviron. Engng ASCE* **135**, No. 10, 1404–1418.

Yamashita, S., Kawaguchi, T., Nakata, Y., Mikami, T., Fujiwara, T. & Shibuya, S. (2009). Interpretation of international parallel test on the measurement of G_{max} using bender elements. *Soils Found*. **49**, No. 4, 631–650.

Yang, J. (2002). Liquefaction resistance of sand in relation to P-wave velocity. *Géotechnique* **52**, No. 4, 295–298, http://dx.doi.org/10.1680/geot.2002.52.4.295.

Yang, J. & Gu, X. Q. (2010). Dynamic shear modulus of dry sand: effect of test method. *Proc. 14th Eur. Conf. on Earthquake Engng, Ohrid*, paper 368 (CD-ROM).